ChemComm

COMMUNICATION

View Article Online
View Journal | View Issue

Cite this: *Chem. Commun.*, 2015, 51, 9173

Received 21st December 2014,
Accepted 23rd April 2015

DOI: 10.1039/c4cc10209f

www.rsc.org/chemcomm

Highly reliable switching *via* phase transition using hydrogen peroxide in homogeneous and multi-layered $GaZnO_x$-based resistive random access memory devices†

Sung Pyo Park, Doo Hyun Yoon, Young Jun Tak, Heesoo Lee and Hyun Jae Kim*

Here, we propose an effective method for improving the resistive switching characteristics of solution-processed gallium-doped zinc oxide ($GaZnO_x$) resistive random access memory (RRAM) devices using hydrogen peroxide. Our results imply that solution processed $GaZnO_x$ RRAM devices could be one of the candidates for the development of low cost RRAM.

Conventional nonvolatile flash memory has been extensively studied in recent years due to its low fabrication cost and density comparable to that of 2X nm generations. However, flash memory still suffers from limitations such as low endurance, low write speed, and high voltage requirements for write operations.[1] In addition, the downscaling of flash memory is expected to reach physical limits in near future due to retention degradation. When the tunnelling oxide thickness is less than 10 nm, stored charges of the floating gate easily escape because of defects in the tunnelling oxide, formed by repeated write/erase operations or direct tunnelling current.[2] Hence, resistive random access memory (RRAM) based on reversible resistive switching (RS) behaviour has been extensively studied for use in next-generation nonvolatile data-storage devices.[2–5] Many candidate materials have been reported for RRAM devices, including transition metal oxides (TMOs), perovskites such as $Pr_{0.7}Ca_{0.3}MnO_3$ and $SrZrO_3$, amorphous silicon, organic and inorganic materials.[3–9] Among these materials, TMOs are promising candidates as they exhibit reliable and stable switching, improved high resistance state to low resistance state (HRS/LRS) ratios, high endurance, and complementary metal oxide semiconductor (CMOS) process compatibility.[10,11] In particular, zinc oxide (ZnO) based TMOs have been actively investigated since they are considered to be environmentally friendly,[12] exhibit a large HRS/LRS ratio, are transparent and flexible, and their raw materials are available in natural abundance.[13,14] Gallium-doped zinc oxide ($GaZnO_x$) has shown particular promise recently for its low cost and thermal stability.[15] $GaZnO_x$ can be fabricated using various techniques including atomic layer deposition,[16] pulse laser deposition,[17] sputtering,[18] and a solution process.[19] The solution process has a number of advantages, including the simplicity of the process, easy control of substances, low cost, and selective deposition.[20] Among the solution process technologies, however, the spin coating method requires repeated processing to achieve optimized active layer thickness, which may result in interface barriers between active layers that affect the RS characteristics of the RRAM device. Also, solution processed TMOs contain intrinsic oxygen vacancies, denoted V_O, which may be shown through a filament model to form a conduction path in storage media.[21] Among switching mechanism models, the widely used nanoscale conductive V_O filament model shows applicability to an extensive range of materials and compares well to experimental measurements;[21] use of this model has demonstrated that control of oxygen species (oxygen and V_O) is necessary for improving RS characteristics. Also, reducing the number of V_O filaments assists in lowering the RESET current and raising the resistance. Many studies have been undertaken to ameliorate these problems *via* doping, post-treatment, and development of multi-layer structures.[2,22,23] In this communication, we propose an effective method for controlling V_O concentrations, and investigate the phenomenon of phase transition using hydrogen peroxide (H_2O_2) in solution processed $GaZnO_x$ RRAM devices with a homogeneous multi-layered (HML) structure. Aluminum and heavily doped p-type silicon (p^+Si) were used for the top and bottom electrodes, respectively; these are conventional materials in microelectronics systems, and serve as a good integration platform. Lastly, we studied the correlation between switching behavior and the material phase of $GaZnO_x$ by varying the deposition location of H_2O_2 treated $GaZnO_x$: pristine, top (top treatment), middle (middle treatment), and bottom (bottom treatment). Detailed experimental conditions and steps are provided in the ESI.† Fig. 1 shows the atomic percentage with depth for each H_2O_2-treated $GaZnO_x$ thin film according to deposition location: pristine 1(a), top 1(b), middle 1(c), and bottom deposition 1(d), analyzed using X-ray photoelectron spectroscopy (XPS). XPS spectra were

School of Electrical and Electronic Engineering, Yonsei University, 50 Yonsei-ro, Seodaemun-gu, Seoul 120-749, Republic of Korea. E-mail: hjk3@yonsei.ac.kr; Fax: +82-2-2123-8123; Tel: +82-2-2123-5865

† Electronic supplementary information (ESI) available. See DOI: 10.1039/c4cc10209f

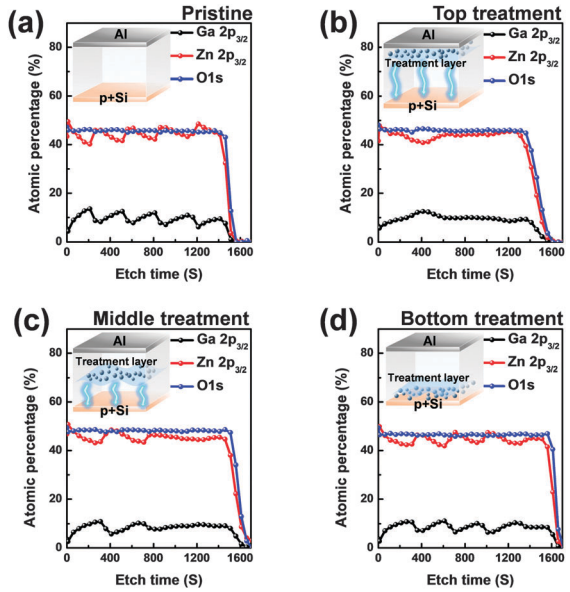

Fig. 1 XPS depth profiles to observe composition variations according to deposition location of H_2O_2-treated $GaZnO_x$ thin films for (a) pristine, (b) top treatment, (c) middle treatment, and (d) bottom treatment (the inset image shows the schematic of the deposition location of the H_2O_2-treated $GaZnO_x$ thin film).

obtained using an Al monochromated X-ray source (Al Kα line: 1486.6 eV). The etch rate of the XPS depth analysis was 0.15 nm s^{-1} using ionic Ar at 1 keV. We observed that atomic percentages of Ga and Zn fluctuate periodically in the pristine $GaZnO_x$ film with increasing etch time, as shown in Fig. 1(a). These results suggest that the Ga and Zn composition in the multi-layered pristine $GaZnO_x$ thin film is segregated at the interfaces during the pre-annealing process, since the film was formed using five repeated processes to optimize the thickness (four times for each pristine $GaZnO_x$ sub-layer and once for H_2O_2-embedded $GaZnO_x$). This segregation may derive from doping inefficiencies or from the maximum solubility of Ga.[24] The segregated phase at the interface can affect the formation and rupture of V_O filaments, which degrades the electrical characteristics of a RRAM device. The top-treated $GaZnO_x$ thin film, however, showed smooth atomic Ga and Zn percentages, as shown in Fig. 1(b). These results indicate the effect of H_2O_2 on HML $GaZnO_x$ thin films. XPS depth profiles were also measured for the other deposition locations (middle and bottom). Fig. 1(c) and (d) clearly shows smooth Ga and Zn atomic percentages, blended by the H_2O_2 treatment. This implies that atomic arrangement varies for $GaZnO_x$ treated with H_2O_2 when compared with the pristine $GaZnO_x$ thin film. Fig. 2(a) and (b) show the XPS depth spectra for Ga $2p_{3/2}$ and Zn $2p_{3/2}$ peaks, for both H_2O_2-treated $GaZnO_x$ and the non-treated $GaZnO_x$ region in the middle-treated $GaZnO_x$ thin film. Each spectrum was deconvoluted using a Gaussian distribution after correcting for background. The Ga $2p_{3/2}$ and Zn $2p_{3/2}$ spectra were centered at 1118.77 eV and 1022.21 eV, respectively, corresponding to GaO and ZnO.[25,26] As shown in Fig. 2(a) and (b), the Ga $2p_{3/2}$ and Zn $2p_{3/2}$ peaks shift to higher binding energy in the H_2O_2-treated $GaZnO_x$ region, suggesting that the GaO–ZnO film formed not just as a

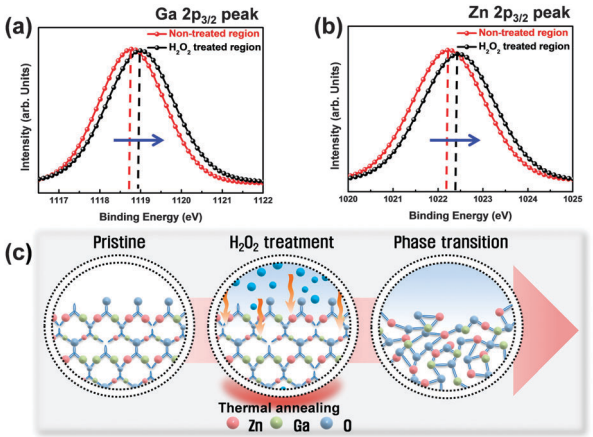

Fig. 2 XPS results for (a) Ga $2p_{3/2}$ and (b) Zn $2p_{3/2}$ peaks for middle-treated $GaZnO_x$ thin film (c) schematic of phase transition.

physical mixture with two distinct GaO and ZnO phases, but that an enhanced oxidation state was found in the $GaZnO_x$ system. Based on the above results, the effects of H_2O_2 treatment on the $GaZnO_x$ film can be clearly seen. Oxygen radical diffusion by H_2O_2 dissociation may affect the $GaZnO_x$ phase during pre-annealing. These results are consistent with the study by Tsai *et al.*,[27] who assumed that the phase of the ZnO film can be changed from polycrystalline to amorphous-like by penetration of dissociated oxygen radicals. Fig. 2(c) shows the phase transition and blended arrangement of Ga and Zn due to H_2O_2 treatment schematically, after 300 °C pre-annealing. To verify the phase transition and crystallinity of H_2O_2-treated $GaZnO_x$ films by oxygen radical diffusion, we compared the H_2O_2-treated $GaZnO_x$ film with the pristine $GaZnO_x$ film using grazing incidence X-ray diffraction (GIXRD), with a 3 kW sealed X-ray tube Cu Kα (λ = 1.541 Å), as shown in Fig. 3. For the pristine $GaZnO_x$ film, XRD analysis revealed no diffraction peaks, implying the amorphous phase. However, the H_2O_2-treated $GaZnO_x$ film was found to be in the *c*-axis oriented polycrystalline phase, with the highest peak observed at 34.48°,[28] indicating a $GaZnO_x$ phase transition instigated by H_2O_2 treatment. Overall, the H_2O_2-induced phase transition correlates well with the results of the previous study in terms of oxygen radical diffusion.[27]

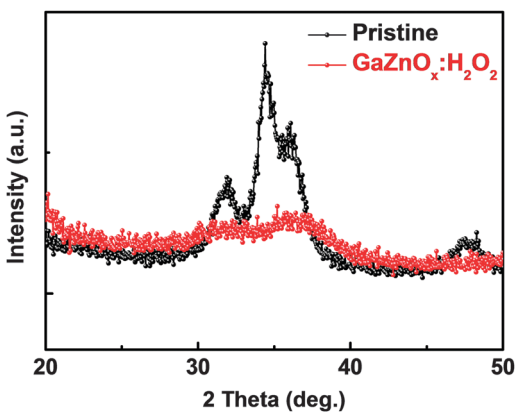

Fig. 3 Grazing incidence X-ray diffraction patterns of $GaZnO_x$ thin films with and without H_2O_2.

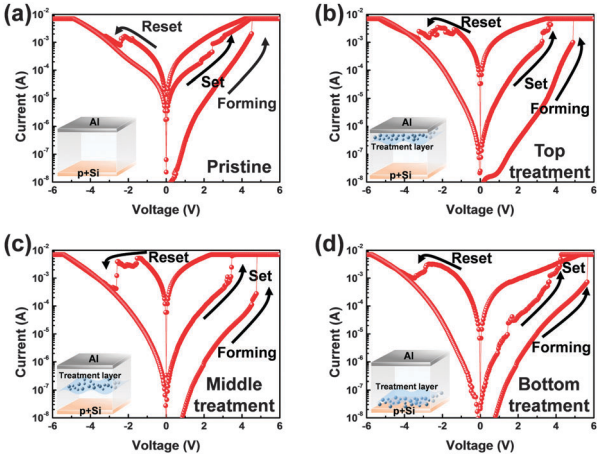

Fig. 4 *I–V* characteristics of the HML structure RRAM devices for (a) pristine, (b) top treatment, (c) middle treatment, and (d) bottom treatment.

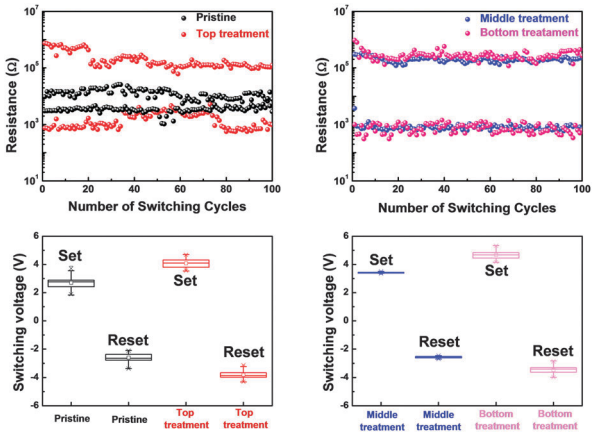

Fig. 5 Comparison of endurance characteristics and SET/RESET voltage distribution of the HML structure RRAM devices.

We analyzed the electrical characteristics of all devices to investigate the effect of H_2O_2 treatment on HML $GaZnO_x$ RRAM devices. Fig. 4 shows the current–voltage (*I–V*) characteristics of the devices according to the deposition location. All devices show clear BRS characteristics. This bi-stable switching is due to the formation and rupture of V_O filaments.[21] The bottom electrode was ground, and a bias voltage (positive and negative) was applied to the top electrode for switching the device. When a sweep voltage ranging from zero to positive was applied to the top electrode of the pristine $GaZnO_x$ device, a sudden decrease in resistance from HRS to LRS (defined as the SET process) was observed at about +2.43 V. As the applied voltage swept from positive to zero, LRS was maintained. Sweeping from zero to negative, an increase in resistance from LRS to HRS (defined as the RESET process) was observed at about −2.19 V. As the applied voltage swept from negative to zero, HRS was maintained. The current was limited to 7 mA during the high-to-low and low-to-high resistance switching processes to avoid permanent damage to the devices. The pristine $GaZnO_x$-based device exhibited poor BRS characteristics as shown in Fig. 4(a). There are two possible explanations; the first is the generation of excess intrinsic V_O in the solution processed $GaZnO_x$ thin film. Since the formation and rupture of conduction filaments (CFs) are attributed to V_O, appropriate control of V_O in TMO-based RRAM is a necessity. Therefore, excess intrinsic V_O induces poor switching characteristics. The second explanation is that nanocrystalline grain boundaries in pristine $GaZnO_x$ cause non-uniform switching characteristics. Grain boundaries are known to be preferential sites for V_O filament formation, it is therefore commonly accepted that excess electrical conduction paths might form due to the high number of grain boundaries in the nanocrystalline $GaZnO_x$ thin film.[29] Also, random nucleation and growth of CFs along grain boundaries make their formation difficult to control, which is a significant impediment to device performance improvement. In contrast, top-, middle-, and bottom-treated $GaZnO_x$ devices exhibited an improvement in the switching window (of the order of $\sim 10^2$) as shown in Fig. 4(b)–(d), respectively. For bottom-treated $GaZnO_x$ devices, however, HRS and LRS were shifted toward the low current level and showed a multi-step SET voltage (Fig. 4(d)). This phenomenon is attributed to the $GaZnO_x$/Si interface at the bottom electrode, where a native oxide forms because of the strong oxidation potential of H_2O_2 and large free energy of formation.[30–32] The formation of native oxide at the $GaZnO_x$/Si interface interrupts the generation of uniform CFs and impedes current flow. To compare the electrical stability of devices, we carried out endurance tests at a reading voltage of 0.4 V and plotted SET/RESET distribution during 100 switching cycles, as shown in Fig. 5. With the exception of the pristine device, all devices showed enhanced endurance characteristics up to 100 cycles. However, resistance fluctuations were observed in top and bottom treated $GaZnO_x$ devices, possibly due to the amorphized $GaZnO_x$ phase transition and formation of native oxide at the bottom electrode. Also, the SET and RESET voltages for the top-treated $GaZnO_x$ device were higher than for the middle-treated sample, since H_2O_2 treatment increases the metal-oxide bond in $GaZnO_x$ and causes a material phase change from polycrystalline to amorphous. These results are consistent with middle-treated samples. In contrast, the middle-treated device exhibited a highly uniform SET/RESET distribution compared with other devices. Overall, the middle-treated $GaZnO_x$ device showed better BRS characteristics, including SET/RESET distribution, endurance, and switching window, amongst the four comparison groups. Fig. 6 shows a feasible BRS conduction mechanism for the middle-treated $GaZnO_x$ device. The schematic is based on characteristics resulting from the rupture and formation of conductive V_O filaments at the interfaces between non-treated $GaZnO_x$ and H_2O_2-treated $GaZnO_x$, caused by a redox reaction. When the applied voltage reaches the positive forming voltage to create a conduction path, oxygen ions attracted from the amorphous region move toward the top Al electrode and the V_O simultaneously move downward. Compared with the non-treated $GaZnO_x$ layer, higher densities of lattice and interstitial oxygen ions exist in H_2O_2-treated $GaZnO_x$, hence uniform CFs were formed in the H_2O_2-treated region. Thus, asymmetrically shaped CFs with weak CF offshoots were formed at the interface, causing the device to switch to the LRS. When a negative bias is applied to the top Al electrode, the repelled oxygen ions

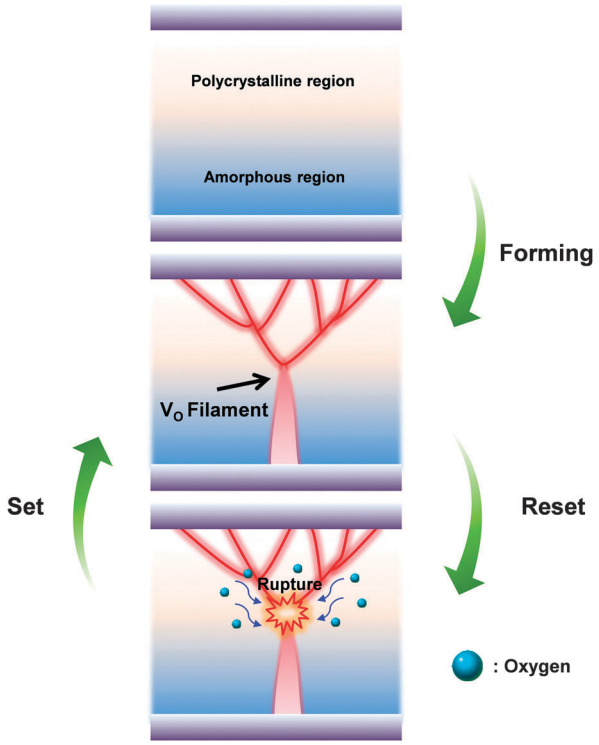

Fig. 6 The conduction mechanism schematic for the BRS in the middle-treated $GaZnO_x$ RRAM device.

from the non-treated polycrystalline region move to the polycrystalline/amorphous interface, where they induce local Joule heating and oxidation. The narrow size of the asymmetric CFs at the interface induces intense local Joule heating, resulting in switching to HRS. This localized interface RS reduces the problem of escape of oxygen ions from electrodes in the middle-treated device.[33] Hence, the middle-treated device showed superb RS characteristics compared with other devices, with improved switching parameters such as SET/RESET distribution, endurance and on/off ratio.

In this communication, we investigated the phase transition of solution-based HML $GaZnO_x$ RRAM devices using H_2O_2 to improve the RS characteristics such as SET/RESET uniformity, endurance, and switching window. Significant variations in *I–V* characteristics were observed, depending on the deposition location of H_2O_2-treated $GaZnO_x$. The pristine $GaZnO_x$ based device exhibited poor BRS characteristics such as large variation in switching voltage, narrow switching window, and poor reproducibility during repeated switching cycles. In contrast, the H_2O_2-treated RRAM devices showed improved BRS characteristics. In particular, the middle-treated device exhibited a high LRS/HRS ratio (of the order of $\sim 10^2$), stable endurance, and narrow dispersion of SET/RESET switching voltage. These results suggest that H_2O_2-treated $GaZnO_x$ solution both assisted physical mixing in the segregated material system, and changed the material phase from polycrystalline to amorphous in pristine $GaZnO_x$ layers. Furthermore, H_2O_2 effectively smoothens interfaces *via* diffusion of oxygen radicals dissociated from H_2O_2 in solution-based HML $GaZnO_x$ RRAM devices. Solution based HML $GaZnO_x$ RRAM devices using H_2O_2 therefore enable the realization of low-cost portable electronics.

This work was supported by the National Research Foundation of Korea (NRF) grant funded by the Korea government (MSIP) [No. 2011-0028819].

Notes and references

1 S. Tehrani, J. M. Slaughter, E. Chen, M. Durlam, J. Shi and M. DeHerrera, *IEEE Trans. Magn.*, 1999, **35**, 2814.
2 D. H. Yoon, S. J. Kim, J. Jung, H. S. Lim and H. J. Kim, *J. Mater. Chem.*, 2012, **22**, 17568.
3 B. Sun, W. Zhao, L. Wei, H. Li and P. Chen, *Chem. Commun.*, 2014, **50**, 13142.
4 M. J. Rozenberg, I. H. Inoue and M. J. Sánchez, *Phys. Rev. Lett.*, 2004, **92**, 178302.
5 M. C. Wu, W. Y. Jang, C. H. Lin and T. Y. Tseng, *Semicond. Sci. Technol.*, 2012, **27**, 065010.
6 B. M. Köpe, M. Tendulkar, S. G. Park, H. D. Lee and Y. Nishi, *Nanotechnology*, 2011, **22**, 254029.
7 S. H. Jo, K.-H. Kim and W. Lu, *Nano Lett.*, 2008, **9**, 496.
8 C.-J. Jung, J.-H. Wu and G.-S. Liou, *Chem. Commun.*, 2014, **50**, 4335.
9 F. Pan, S. Gao, C. Chen, C. Song and F. Zeng, *Mater. Sci. Eng., R*, 2014, **83**, 1–59.
10 W. Y. Chang, Y. C. Lai, T. B. Wu, S. F. Wang, F. Chen and M. J. Tsai, *Appl. Phys. Lett.*, 2008, **92**, 022110.
11 H. Lv, X. Xu, H. Liu, R. Liu, Q. Liu, W. Banerjee, H. Sun, S. Long, L. Li and M. Liu, *Sci. Rep.*, 2015, **5**, 7764.
12 F. Tamaddon, M. A. Amrollahi and L. Sharafat, *Tetrahedron Lett.*, 2005, **46**, 7841.
13 Y. C. Yang, F. Pan, Q. Liu, M. Liu and F. Zeng, *Nano Lett.*, 2009, **9**, 1636.
14 Z. Q. Wang, H. Y. Xu, X. H. Li, X. T. Zhang, Y. X. Liu and Y. C. Liu, *IEEE Electron Device Lett.*, 2011, **32**, 1442.
15 B. D. Ahn, S. H. Oh, H. J. Kim, M. H. Jung and Y. G. Ko, *Appl. Phys. Lett.*, 2007, **91**, 252109.
16 S. J. Lim, S. J. Kwon, H. Kim and J. S. Park, *Appl. Phys. Lett.*, 2007, **91**, 183517.
17 H. Frenzel, A. Lajn, M. Brandt, H. von Wenckstern, G. Biehne, H. Hochmuth, M. Lorenz and M. Grundmann, *Appl. Phys. Lett.*, 2008, **92**, 192108.
18 Y. J. Tak, D. H. Yoon, S. Yoon, U. H. Choi, M. M. Sabri, B. D. Ahn and H. J. Kim, *ACS Appl. Mater. Interfaces*, 2014, **6**, 6399.
19 C. H. Kim, Y. S. Rim and H. J. Kim, *ACS Appl. Mater. Interfaces*, 2013, **5**, 6108.
20 S. J. Heo, D. H. Yoon, T. S. Jung and H. J. Kim, *J. Inf. Disp.*, 2013, **14**, 79.
21 N. Xu, L. Liu, X. Sun, X. Liu, D. Han, Y. Wang, R. Han, J. Kang and B. Yu, *Appl. Phys. Lett.*, 2008, **92**, 232112.
22 D. H. Yoon, Y. J. Tak, S. P. Park, J. Jung, H. Lee and H. J. Kim, *J. Mater. Chem. C*, 2014, **2**, 6148.
23 Y. Bai, H. Wu, Y. Zhang, M. Wu, J. Zhang, N. Deng, H. Qian and J. Yu, *Appl. Phys. Lett.*, 2013, **102**, 173503.
24 J. A. Sans, G. M. Criado, J. P. Porres, J. F. S. Royo and A. Segura, *Appl. Phys. Lett.*, 2007, **91**, 221904.
25 T. Das, C. Mahata, C. K. Maiti, E. Miranda, G. Sutradhar and P. K. Bose, *Appl. Phys. Lett.*, 2011, **98**, 022901.
26 J. L. Lan, S. J. Cherng, Y. H. Yang, Q. Zhang, S. Subramaniyan, F. S. Ohuchi, S. A. Jenekhe and G. Cao, *J. Mater. Chem. A*, 2014, **2**, 9361.
27 C. H. Tsai, W. C. Wang, F. L. Jenq, C. C. Liu, C. I. Hung and M. P. Houng, *J. Appl. Phys.*, 2008, **104**, 053521.
28 W. J. Park, H. S. Shin, B. D. Ahn, G. H. Kim, S. M. Lee, K. H. Kim and H. J. Kim, *Appl. Phys. Lett.*, 2008, **93**, 083508.
29 M. Lanza, K. Zhang, M. Porti, M. Nafría, Z. Y. Shen, L. F. Liu, J. F. Kang, D. Gilmer and G. Bersuker, *Appl. Phys. Lett.*, 2012, **100**, 123508.
30 J. M. Kwon, J. Jung, Y. S. Rim, D. L. Kim and H. J. Kim, *ACS Appl. Mater. Interfaces*, 2014, **6**, 3371.
31 R. Waser, R. Dittmann, G. Staikov and K. Szot, *Adv. Mater.*, 2009, **21**, 2632.
32 Y. T. Chen, T. C. Chang, H. K. Peng, H. C. Tseng, J. J. Huang, J. B. Yang, A. K. Chu, T. F. Young and S. M. Sze, *Appl. Phys. Lett.*, 2013, **102**, 252902.
33 D. Acharyya, A. Hazra and P. Bhattacharyya, *Microelectron. Reliab.*, 2014, **54**, 541.

